Nonlinear Interference Noise in Raman-amplified WDM Systems

Francesco Lorenzi(*), Gianluca Marcon, Andrea Galtarossa *Fellow, IEEE*, *Fellow, OPTICA*, Luca Palmieri *Member, IEEE*, Antonio Mecozzi *Fellow, IEEE*, *Fellow, OPTICA*, Cristian Antonelli *Senior Member, IEEE*, *Fellow, OPTICA*, Marco Santagiustina *Member, IEEE*

***Abstract*—Raman amplification is a solution for broadband wavelength-division multiplexed (WDM) systems that require fine and reconfigurable gain tuning. However, as the fiber nonlinearity ultimately limits the performance of fiber-optic communication systems, accurate models of the nonlinear interference affecting signal propagation in the presence of multiple Raman pumps are critical for system design. In this study, we propose an extension of the time-domain nonlinear interference noise (NLIN) model for analyzing Raman-amplified polarization multiplexed WDM links. Our proposed model enables the evaluation of the NLIN power and inter-channel power transfer induced by stimulated Raman scattering (SRS) in systems with Raman-gain equalization. It also accounts for the evolution of the average signal power along the link, which varies from channel to channel. To compute the noise contributions efficiently, we employ a method that enables us to apply the model in three relevant pumping scenarios: co-propagating, counter-propagating, and bidirectional pumping. Using the model, we evaluate the differences in NLIN power over all the channels. Additionally, we can estimate the amplified stimulated emission power, which can be used to optimize the optical signal-to-noise ratio with respect to the input signal and pump powers.**

***Index Terms*—Fiber nonlinear optics, nonlinear interference, optical fiber communication, Raman amplification, WDM.**

I. Introduction

MANY aspects of nonlinear impairments in optical communication systems have been thoroughly studied in recent years, and various mitigation methods have been proposed. The majority of these methods leverage the digital signal processing (DSP) capabilities, that are readily available in modern digital coherent receiver [1], for compensating physical impairments. The performance of fiber-optic systems is known to be ultimately bounded by the fiber nonlinearity, and this limit is often referred to as the nonlinear Shannon limit [2–4].

In practical systems, the nonlinear interference between frequency channels induced by the fiber Kerr effect can be conveniently modeled in the form of additive noise, referred to as the nonlinear interference noise (NLIN) [5, 6]. The NLIN has been well described by a modulation-format dependent non-linear phase noise (NLPN), plus a residual noise [5, 7]. In long-haul dispersion-uncompensated systems, the NLPN exhibits long auto-correlation times, that allow for efficient filtering of this noise contribution. This effect has been characterized in recent experiments [8–10], and filtering techniques based on auto-regressive and Kalman filtering have been investigated [11].

The direct calculation of the NLIN through split-step simulations is computationally time-consuming, so it is preferable to refer to simpler analytical or semi-analytical models. Many of them have been developed in the frequency-domain (FD) under the assumption of Gaussian noise and signals, as in the well-known Gaussian noise (GN) model [12, 13]. In its original formulation, the GN model does not account for the modulation format-dependence of NLIN, but it was rapidly expanded in subsequent works, under the name of enhanced Gaussian noise (EGN) model [14, 15].

In parallel to the development of FD models derived from the GN, a time-domain (TD) approach accounting also for the dependence of the NLIN on the modulation format of the transmitted signal, has been proposed in [4, 7, 16]. This model treats the Kerr nonlinearity as a perturbation in the nonlinear Schrödinger equation (NLSE), and assumes a matched filter-based coherent reception scheme in chromatic-dispersion uncompensated systems.

In this work we focus on the evaluation of the NLIN in Raman amplified links (RALs), whose typical span reach is in the range of 100 km. To this end, we use the TD model introduced in [16] and its extension to the case of polarization-multiplexed transmission [5, 17], and generalize it to account for the dependence of the gain/loss profile on propagation distance determined by the Raman amplification, as well as for its channel-to-channel variations. Indeed, in RALs the signal power evolution is not, in general, the same for all the channels, and depends on the other channels and pumps evolution in a nonlinear way. The present extension of the NLIN model addresses the scenario of RALs in which an optimization of the total link gain is performed. In particular, for Raman amplification equalization, we will exploit the method introduced in [18] that is also extended to treat three relevant pumping schemes [19]: co-propagating, counter-propagating and bidirectional pumping. In this work we focus on the analysis of cross-phase modulation (XPM), which is the predominant nonlinear distortion mechanism, and derive an expression for the NLIN variance extending the

Francesco Lorenzi is with the Department of Physics and Astronomy, University of Padova, 35131 Padova, Italy (* e-mail: francesco.lorenzi.2@phd.unipd.it). Gianluca Marcon, Andrea Galtarossa, Luca Palmieri, and Marco Santagiustina are with the Department of Information Engineering, University of Padova, 35131 Padova, Italy, and also with CNIT – National Inter-University Consortium for Telecommunications. Cristian Antonelli and Antonio Mecozzi are with the Department of Physical and Chemical sciences, University of L'Aquila, 67100 L'Aquila, and also with CNIT – National Inter-University Consortium for Telecommunications.

approach of [16]. The presented model also accounts for the accumulation of modulation-format-dependent noise produced by inter-channel stimulated Raman scattering noise (SRSN), a problem that was addressed in [20–22].

The article is organized as follows. In section II, we review the Raman model for pump optimization and present the extended model for NLIN, which is the main contribution of this work. Following a similar argument as in the model for NLIN, we present also a method for computing SRSN. In section III, we present extensive numerical results on the evaluation of all the noise contributions, that are NLIN, SRSN, and amplified spontaneous emission (ASE), for three different Raman pumping schemes, namely, co-propagating, counter-propagating, and bidirectional pumping. We analyze the results by comparing different signal input powers and channel wavelengths inside the WDM spectrum. The optimal signal input power is found for each pumping scheme.

II. NLIN AND SRSN MODEL

A. Raman model

In this work, we leverage on an optimization routine for pump placement based on a machine learning algorithm that was developed for Ramam gain equalization in few-mode fibers [18]. One of the remarkable features of that scheme is that it is based on the physical model of the Raman interaction, i.e. it includes the depletion of the pumps and the signal-to-signal amplification. Hence, our work is different from [21], where approximated solutions were used for the pump and signal evolution to derive a closed formula. The physical model underlying the optimization routine is the system of differential equation of the average wave powers [19, 23] as briefly reviewed in the following. Let the total number of pumps and signals be denoted by $M = M_S + M_P$, of which M_S are signals and M_P are pumps. Let $P_i(z)$, with $i \in \{1, ..., M\}$ be the power of the i-th wave, and use the superscript $+$ or $-$ to denote waves co-propagating or counter-propagating with the signals. Let $C_R(\lambda_i, \lambda_j)$ be the Raman gain coefficient between waves i and j, which depends on the Raman gain spectrum of silica g_R and the effective area A_{eff}. Finally, let α_i be the fiber attenuation coefficient at wavelength λ_i. A steady-state profile for the power of the waves must satisfy the following system of equations:

$$\pm\frac{\mathrm{d}P_i^{\pm}}{\mathrm{d}z} = -\alpha_s P_i^{\pm} + \left[\sum_{j\neq i} C'_{i,j}\left[P_j^{+} + P_j^{-}\right]\right] P_i^{\pm}, \quad (1)$$

with the Raman coefficient defined by

$$C'_{i,j} = \begin{cases} C_R\left(\lambda_i, \lambda_j\right) & \text{if } \lambda_i > \lambda_j \\ -\frac{\lambda_i}{\lambda_j} C_R\left(\lambda_j, \lambda_i\right) & \text{if } \lambda_i < \lambda_j \end{cases}. \quad (2)$$

Eqs. 1 allow us to describe the interaction between all waves in the same way, therefore, as stressed before, the model includes effects such as signal-to-signal and pump-to-pump power exchange, so it is suitable to describe higher-order pumping schemes. The system of equations (1) does not describe amplified spontaneous emission (ASE), that can be modeled as in [19, 23], where ASE-induced depletion of pumps and signals is neglected as it is usually done for realistic systems. This leads to a set of M_S equations for the ASE noise power N_i that accumulates in the band of channel i:

$$\begin{aligned}\frac{\mathrm{d}N_i}{\mathrm{d}z} =& -\alpha_i\, N_i + \left[\sum_{j\neq i} C'_{i,j}\left[P_j^{+} + P_j^{-}\right]\right] N_i \\ &+ \left[\sum_{j\neq i} \eta_{i,j} C'_{i,j}\left[P_j^{+} + P_j^{-}\right]\right] 2\hbar\omega_i B_{\text{ref}},\end{aligned} \quad (3)$$

where $\hbar$ is the reduced Planck constant, ω denotes frequency, B_{ref} is the channel bandwidth, and $\eta_{i,j}$ is the distribution of phonons at thermal equilibrium

$$\eta_{i,j} = \frac{1}{\exp\left[\hbar\left(\omega_i - \omega_j\right)/k_B\theta\right] - 1}, \quad (4)$$

with k_B the Boltzmann constant and θ the absolute temperature. Note that equations (3) can be solved after the computation of the power evolution from Eq. (1).

In this work, the optimization algorithm is set to obtain the optimal pump configuration to achieve a total link gain of −3 dB for all the channels in the C-band, corresponding to approximately 17 dB Raman on-off gain for a 100 km typical fiber link, assuming an attenuation value of 0.2 dB km^{-1} in the center of the C-band. The input data of the optimization routine are the number of channels and their input powers, the band occupation, and the number of co-propagating and counter-propagating pumps, whose wavelength and powers are to be optimized. In particular, the optimization procedure aims at minimizing the average value of the absolute difference between the output channel power and a target power value, where the average is performed over all the wavelength-division multiplexing (WDM) channels. The target power value is assumed to be 3 dB smaller than the launch signal power, a choice that relies on the notion that hybrid amplification, where distributed Raman amplifier (DRA) is followed by an erbium-doped fiber amplifier (EDFA), is in most cases optimal in terms of optical signal-to-noise ratio

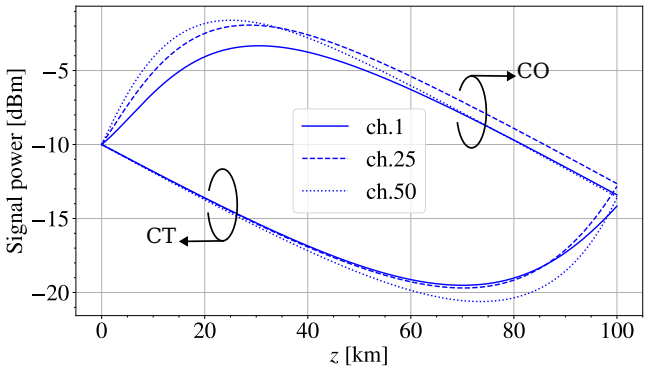

Fig. 1. Evolution of the signal powers of 3 channels for the case of 4 co-propagating pumps (CO) and 4 counter-propagating pumps (CT), for an input power of −10 dBm per channel. The WDM grid occupies a bandwidth of ≈ 5 THz. Channel 50 is at 1558 nm, and channel 1 is at 1600 nm. The evolution of the individual pump powers for the CO case is shown in Fig. (3). The target output power is set to −13 dBm.

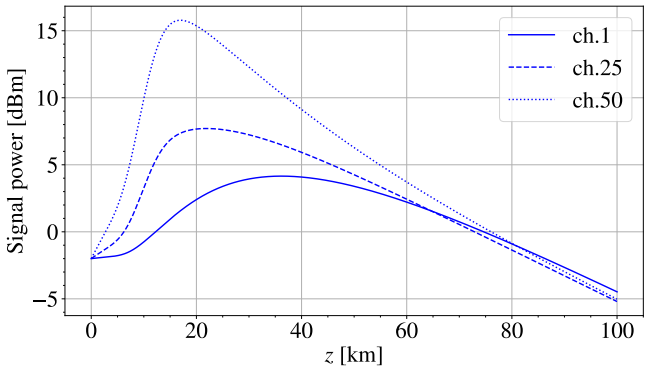

Fig. 2. Evolution of the signal powers of the same 3 channels of Fig. 1, for the case of 4 co-propagating pumps and for an input power of −2 dBm per channel. Pump power evolution shown in Fig. (4). Target output power is set to −5 dBm).

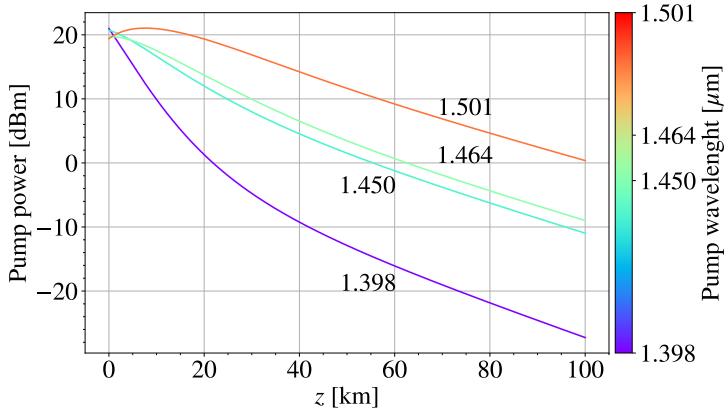

Fig. 3. Evolution of the power of the 4 co-propagating pumps for signal input power of −10 dBm per channel.

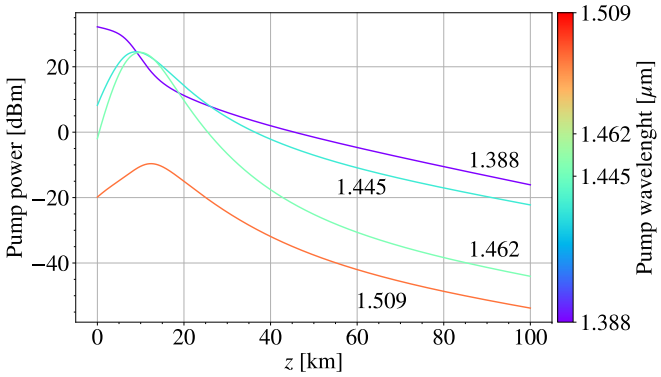

Fig. 4. Evolution of the power of the 4 co-propagating pumps for signal input power of −2 dBm per channel.

(OSNR) [24, 25]. In section III, we calculate the OSNR for several hybrid-configuration settings, and show that full DRA is mildly optimal in terms of NLIN.

Let us stress that including all Raman interactions is critical, in particular in the co-propagating pump regime. Referring to a system composed of 100 km of standard fiber with 50 channels, spaced by 100 GHz in the C-band (5 THz optical bandwidth), and using 4 co-propagating pumps, we obtain the evolution of the power of signals plotted in Fig. 1 for −10 dBm input power, and in Fig. 2 for −2 dBm input power. The power evolution of three representative channels (longest, shortest, and middle wavelength) is shown. In Figs. 3 and 4, the power evolution of the pumps for the same cases are represented for comparison. In the −2 dBm case, Fig. 2 shows that shorter wavelength channels are amplified to reach powers of the same order of magnitude of the pumps (about 15 dBm) but then are depleted in the middle of the link; in fact, it can be observed that the negative slope (e.g. channel 50) is greater than that due to fiber attenuation. This suggests that lower wavelength channels contribute to the total gain of longer wavelength channels, through a cascaded Raman amplification. Cascaded Raman amplification is also clearly affecting the evolution of the pumps as shown in Fig. 4. This effect can be so relevant that the optimization algorithm practically switches off the longest wavelength pump (red curve of Fig. 4 at 1.509 μm) which could be in principle eliminated with little changes in the final results. Instead, for the case of −10 dBm input power per channel (Fig. 1), the power dynamics are similar in all the channels and cascading effects are also less pronounced in the pump evolution shown in Fig. 3.

In Fig. 5 we present the values of the input powers of the pumps, as a function of the signal input power per channel, obtained by the optimization for three different pumping schemes, CO, CT, and BI, that correspond respectively to 4 co-propagating pumps, 4 counter-propagating pumps, and the bidirectional case with 2 co- and 4 counter-propagating pumps. For CT and BI pumping the input pump powers of the pumps need to be changed very little as a function of the signal input power (there is a little increase for signal input powers larger than −5 dBm). Similar behavior is observed for the CO scheme up to about −8 dBm; beyond that threshold the power dynamics among pumps and signals, as previously remarked, becomes highly nonlinear, and the optimization procedure, in order to achieve gain equalization, must resort to cascading effects. The high sensitivity to signal input powers and the increase in the total pump power required for the equalization through cascading effects make the high-power CO pumping scheme not convenient. Moreover, as it will be shown in section III, the OSNR is also very low in this regime.

B. NLIN model

The channel model consists of coupled equations derived from the Manakov equation [26], yielding expressions for the NLIN that are similar to those derived in [5]. The main difference is in the fact the power loss profile is channel-specific and follows from the solution of Eqs. 1.

We consider two WDM channels, and denote by A and B the channel of interest and the interfering channel respectively. The quantities $\underline{u}_A(z,t)$ and $\underline{u}_B(z,t)$ are the corresponding slowly-varying complex envelopes, where we use the underline

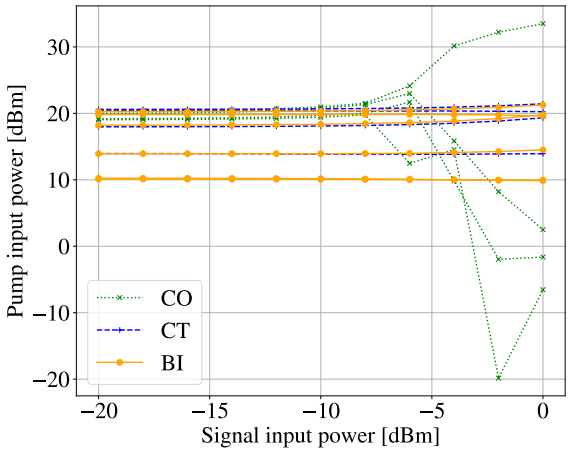

Fig. 5. Pump power as a result of the optimization routine, as a function of signal input power per channel. All target output gains are set to −3 dB. The CO scheme makes use of 4 co-propagating pumps, the CT scheme makes use of 4 counter-propagating pumps, and the BI scheme makes use of 2 co-propagating and 4 counter-propagating pumps. The interpolating lines connect pumps ordered with the same criterion for each input power level.

to denote complex-valued two-dimensional column vectors. At the fiber input, they can be expressed as

$$\begin{aligned}\underline{u}_A(0,t) &= \sum_k \underline{a}_k g(0,t-kT),\\ \underline{u}_B(0,t) &= \sum_k \underline{b}_k g(0,t-kT),\end{aligned} \tag{5}$$

where by $\underline{a}_k$ and $\underline{b}_k$ we denote the k-th symbols transmitted in the x and y polarizations of the two WDM channels respectively, and where T is the symbol time duration. The propagated fundamental pulse waveform $g(z,t)$, is normalized such that

$$\int_{-\infty}^{+\infty} |g(z,t)|^2 dt = 1. \tag{6}$$

Under the assumption of an ideal coherent receiver with matched filtering and dispersion compensation, within the perturbation approach the NLIN affecting the symbol $\vec{a}_0$ can be expressed as follows [16, 17],

$$\begin{aligned}\Delta\underline{a}_0 =& i\frac{8}{9}\gamma \sum_{h,k,m} S_{h,k,m}\underline{a}_k^\dagger \underline{a}_m \ \underline{a}_h\\ &+ i\frac{8}{9}\gamma \sum_{h,k,m} X_{h,k,m}\left(\underline{b}_k^\dagger \underline{b}_m \mathrm{I} + \underline{b}_m \underline{b}_k^\dagger\right) \ \underline{a}_h,\end{aligned} \tag{7}$$

where I is the identity matrix, γ is the fiber nonlinearity coefficient, and by the dagger we denote the Hermitian conjugate. The terms involving the coefficients $S_{h,k,m}$ result from intra-channel nonlinear interference, which is typically assumed to be compensated at the receiver by means of ideal back-propagation or predistortion, and therefore are neglected in what follows [16]. The terms involving the coefficients $X_{h,k,m}$ describe inter-channel nonlinear interference and, among them, the ones with $h = 0$ and $k = m$ are dominant. According to jargon introduced in [17], these terms describe collisions between two pulses, one propagating in the channel of interest and the other in the interfering channel [16]. By restricting ourselves to the considaration of these terms only, the NLIN expression simplifies to

$$\Delta\underline{a}_0 \approx i\gamma\frac{4}{3}\underline{a}_0 \sum_m \|\underline{b}_m\|^2 X_{0,m,m}. \tag{8}$$

The evaluation of the coefficients $X_{0,m,m}$ starts from the Manakov equation

$$\frac{\partial \underline{U}}{\partial z} = -\frac{\hat{\alpha}-\hat{r}}{2}\underline{U} - i\frac{\beta_2}{2}\frac{\partial^2 \underline{U}}{\partial t^2} + i\frac{8}{9}\gamma\|\underline{U}\|^2\underline{U}, \tag{9}$$

where the effects of attenuation and Raman pumping are described by means of the operators $\hat{\alpha}$ and $\hat{r}$, respectively. By expressing $\underline{U}$ as the sum of two signals frequency-spaced by Ω, namely $\underline{U} = \underline{U}_A + \exp(-i\Omega t)\underline{U}_B$, the Manakov equation can be recast in a set of coupled equations for $\underline{U}_A$ and $\underline{U}_B$, where the operators $\hat{\alpha}$ and $\hat{r}$ reduce to frequency-dependent scalar functions of z. In particular, by defining the function $f_j(z)$ as

$$f_j(z) = \exp\left[-\int_0^z (\alpha_j - r_j)\mathrm{d}z'\right] \qquad j = A, B, \tag{10}$$

and by introducing the normalized field vectors $\underline{u}_j$, defined through $\underline{U}_j = \sqrt{f_j(z)}\underline{u}_j$, one finds

$$\begin{aligned}\frac{\partial \underline{u}_A}{\partial z} =& -i\frac{\beta_2}{2}\frac{\partial^2 \underline{u}_A}{\partial t^2}\\ &+ i\frac{8}{9}\gamma\left[f_A(z)\|\underline{u}_A\|^2 + f_B(z)(\|\underline{u}_B\|^2 + \underline{u}_B\underline{u}_B^\dagger)\right]\underline{u}_A,\end{aligned} \tag{11}$$

$$\begin{aligned}\frac{\partial \underline{u}_B}{\partial z} =& -\beta_2\Omega\frac{\partial \underline{u}_B}{\partial t} - i\frac{\beta_2}{2}\frac{\partial^2 \underline{u}_B}{\partial t^2}\\ &+ i\frac{8}{9}\gamma\left[f_B(z)\|\underline{u}_B\|^2 + f_A(z)(\|\underline{u}_A\|^2 + \underline{u}_A\underline{u}_A^\dagger)\right]\underline{u}_B.\end{aligned} \tag{12}$$

The coupled equations yield the following expression for the pulse-collision coefficients,

$$\begin{aligned}X_{0,m,m} =& \int_0^L dz f_B(z)\int_{-\infty}^{+\infty} dt\\ &\times |g^{(0)}(z,t)|^2 |g^{(0)}(z, t-mT-\beta_2\Omega z)|^2,\end{aligned} \tag{13}$$

which can be seen to be real-valued therefore suggesting that the NLIN can be expressed in the form of NLPN, that is $\Delta\underline{a}_0 \approx i\Delta\theta\,\underline{a}_0$. Its variance can be obtained as detailed in [16],

$$\langle\Delta\theta^2\rangle = \frac{16}{9}\gamma^2\left(\langle\|\underline{b}_0\|^4\rangle - \langle\|\underline{b}_0\|^2\rangle^2\right)\sum_m X_{0,m,m}^2, \tag{14}$$

where by the symbol $\langle\cdot\rangle$ we denote ensemble averaging with respect to the distribution of the constellation symbols, and by $\|\underline{u}\|$ the norm of vector $\underline{u}$. The NLPN variance can also be expressed as

$$\langle\Delta\theta^2\rangle = \frac{16}{9}\gamma^2(P_{B,0}T)^2\mu\sum_m X_{0,m,m}^2, \tag{15}$$

where $P_{B,0} = \langle \|\underline{b}_0\|^2 \rangle / T$ is the average channel transmit power, and where by μ we denote the constellation kurtosis given by

$$\mu = \frac{\langle \|\underline{b}_0\|^4 \rangle}{\langle \|\underline{b}_0\|^2 \rangle^2} - 1. \tag{16}$$

Note that μ vanishes for pure phase-modulated signals, such as $M-$PSK, whereas in the case of QAM signals it increases with the modulation order [16]. In the case of multiple WDM channels, the total NLPN variance is obtained by summing the individual contributions, assuming statistical independence between symbols transmitted in different WDM channels.

It is worth noting that the time correlation of the NLPN can be exploited for devising NLPN mitigation schemes based on phase-recovery algorithms [27, 28]. Previous works have shown that the removal of this noise component can be highly effective in long-haul systems, where the NLPN remains correlated over long time intervals, and various phase recovery algorithms, such as the Viterbi and Viterbi algorithm and some of its variants [29], or more sophisticated algorithms [30] have been demonstrated. The situation is different in the case of RALs whose lengths is in the order of 100 km. In these systems the NLPN correlation time is much shorter [5], and therefore effective NLPN compensation is considerably more challenging.

C. SRSN evaluation

The perturbation theory for computing NLIN [16] has been generalized in the previous section, to account for the different channel power evolution, which is a peculiarity of RALs. In this section, we show how the same approach can be applied to account also for channel-to-channel SRS noise. We remark that the set of equations for the pump and signal steady-state powers Eq. (1) can be used also within a time-dependent framework. This is because the wave powers are almost instantaneously affected by the Raman effect since the Raman response is sufficiently broadband with respect to typical single channel bandwidth [26]. In particular, all signal average powers can be substituted with instantaneous powers. Since the signals are always co-propagating, we drop the superscript $+$, and define the instantaneous power as:

$$\tilde{P}_i(z,t) = P_i(z) + \eta_i(z,t), \tag{17}$$

where the $P_i(z)$ are the average powers, i.e. the steady-state profiles utilized in Eq. (1), and $\eta_i(z,t)$ is the time-dependent fluctuation. It is required for the fluctuation to satisfy

$$\langle \eta_i(z,t) \rangle_t = 0, \tag{18}$$

where $\langle \cdot \rangle_t$ denotes the time average, which can be converted to the statistical average for the symbol constellation. Since the channels have independent symbols, one can compute the stimulated Raman scattering (SRS) noise variance in the special case of only two interacting channels A and B, as done before, for NLIN. The propagation equation for $\underline{U}_A$, accounting for the (depolarized) pumps effect, reads

$$\begin{aligned} \frac{\partial \underline{U}_A}{\partial z} =& -\frac{\alpha_A - \tilde{r}_A(z,t)}{2}\underline{U}_A - i\frac{\beta_2}{2}\frac{\partial^2 \underline{U}_A}{\partial t^2} \\ &+ i\frac{8}{9}\gamma(\|\underline{U}_A\|^2 + (\|\underline{U}_B\|^2 + \underline{U}_B\underline{U}_B^\dagger))\underline{U}_A \end{aligned} \tag{19}$$

where we introduced the SRS gain coefficient $\tilde{r}_A(z,t)$, which is now time-dependent. Let $\mathcal{P}_{A,B}$ be the set of all pumps and all signals except A and B. If we denote $r_A(z)$ as the time-averaged Raman contribution due to all channels and pumps, we can write

$$\begin{aligned} \tilde{r}_A(z,t) =& \sum_{j \in \mathcal{P}_{A,B}} C'_{A,j}[P_j^+(z) + P_j^-(z)] \\ &+ C'_{A,B}[P_B(z) + \eta_B(z,t)] \\ =& \, r_A(z) + C'_{A,B}\eta_B(z,t). \end{aligned} \tag{20}$$

The expression for η_B can be obtained by combining results from the steady state analysis, and from the 0^{th} order expression for the propagated field. After the optimization, from the numerical integration of the steady-state Eq. (1) it is possible to obtain $r_A(z)$, and also the term $C'_{A,B}P_B(z)$ separately. The instantaneous power of the channel B can be scaled using the function $f_B(z)$,

$$\begin{aligned} \tilde{P}_B(z,t) &= f_B(z)\|\underline{u}_B(z,t)\|^2 \\ &= f_B(z)\sum_{k,m} \underline{b}_k^\dagger \underline{b}_m g^*(z, t-kT)g(z,t-mT). \end{aligned} \tag{21}$$

The zero-th order fluctuation term $\eta_B^{(0)}(z,t)$ can be obtained from Eq. (17) and Eq. (21) in the following form

$$\eta_B^{(0)}(z,t) = f_B(z)||\underline{u}_B^{(0)}(z,t)||^2 - P_B(z), \tag{22}$$

and its use in the propagation equation of $\underline{u}_A$ yields

$$\begin{aligned} \frac{\partial \underline{u}_A^{(1)}}{\partial z} =& -i\frac{\beta_2}{2}\frac{\partial^2 \underline{u}_A^{(1)}}{\partial t^2} \\ &+ i\frac{8}{9}\gamma\Big[f_A(z)||\underline{u}_A^{(0)}||^2 \\ &+ f_B(z)\left(||\underline{u}_B^{(0)}||^2 + \underline{u}_B^{(0)}\underline{u}_B^{(0)\dagger}\right)\Big]\underline{u}_A^{(0)} \\ &+ \frac{C'_{A,B}}{2}\eta_B^{(0)}(z,t)\underline{u}_A^{(0)}. \end{aligned} \tag{23}$$

The expression for the NLIN is then readily evaluated as follows,

$$\begin{aligned} \Delta\underline{a}_0 =& i\frac{8}{9}\gamma \sum_{h,k,m} S_{h,k,m}\underline{a}_k^\dagger \underline{a}_m \; \underline{a}_h + \\ &+ \sum_{h,k,m}\Big[i\frac{8}{9}\gamma \; X_{h,k,m}\left(\underline{b}_k^\dagger \underline{b}_m \mathrm{I} + \underline{b}_m \underline{b}_k^\dagger\right) \; \underline{a}_h + \\ &+ R_{h,k,m}\underline{b}_k^\dagger \underline{b}_m \mathrm{I} \; \underline{a}_h\Big] - \frac{C'_{A,B}}{2}P_{B,0}\int_0^L dz f_B(z) \; \underline{a}_0, \end{aligned} \tag{24}$$

where the relation $P_B(z) = P_{B,0}f_B(z)$ has been used in the last integral. Note that the last term on the right-hand side of the equality is responsible for a deterministic gain/loss, which turns out to be negligible and therefore is dropped in the analysis that follows. The terms $R_{h,km}$ describe the Raman contribution to the NLIN, and here too we restrict ourselves to the consideration of two pulse collisions only,

which corresponds to the terms with $h = 0$, and $k = m$, whose expression is given by

$$R_{0,m,m} = \frac{C'_{A,B}}{2} \int_0^L dz f_B(z) \int_{-\infty}^{+\infty} dt \times \\ \times |g^{(0)}(z,t)|^2 |g^{(0)}(z, t - mT - \beta_2 \Omega z)|^2. \tag{25}$$

As expected, the SRS contribution to the NLIN is in quadrature with the NLPN. The noise variance due to NLPN and SRSN is therefore given by

$$\langle \|\Delta \underline{a}_0\|^2 \rangle = (P_{A,0}T)\mu(P_{B,0}T)^2 \left| i\frac{4}{3}\gamma + \frac{C'_{A,B}}{2} \right|^2 \sum_m X^2_{0,m,m}, \tag{26}$$

or equivalently

$$\langle \|\Delta \underline{a}_0\|^2 \rangle = (\xi_N + \xi_R)\,(P_{A,0}T)\mu(P_{B,0}T)^2 \sum_m X^2_{0,m,m}, \tag{27}$$

where we defined $\xi_N = 16/9\,\gamma^2$ and $\xi_R = C'^2_{A,B}/4$. In order to estimate the magnitude of SRSN, a comparison between the coefficients ξ_N and ξ_R can be made. The SRSN coefficient ξ_R depends on the frequency shift between channels A and B. In Fig. 6, the strength of the Raman contribution is evaluated for various values of the WDM bandwidth, that sets the maximum frequency shift. An important implication of Fig. 6 is that in the case of C-band transmission (5 THz) considered in this work this noise contribution is negligible, in agreement with the findings of [21].

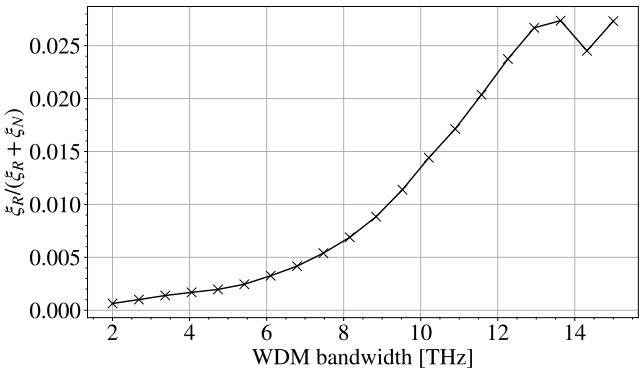

Fig. 6. Magnitude of the maximum SRSN coefficient relative to the sum of ξ_N and ξ_R, as a function of the WDM bandwidth, for two channels at the ends of the considered WDM optical band.

In the section that follows we investigate the dependence of the NLIN variance on the relevant parameters that characterize a typical RAL, by neglecting the contribution of SRSN.

III. Numerical results

The simulation parameters are summarized in Table I. We considered a link of 100 km in which channels are spaced by 100 GHz and the WDM center frequency is 190 THz, so that the channels' frequencies span the range from 187.5 THz to 192.5 THz. The frequency dependence of the fiber attenuation is modeled using a quadratic expansion of the attenuation coefficient with respect to the band center, with typical parameters

TABLE I
Simulation parameters

Parameter	Value
GVD (β_2)	23 ps^2 km^{-1}
NL coefficient γ	1.3 W^{-1} km^{-1}
Effective area (A_{eff})	80 µm^2
Raman coefficient	7×10^{-14} m W^{-1}
Attenuation (at band center)	0.19 dB km^{-1}
Fiber Length (L)	100 km
Baud rate	10 Gbaud
Modulation format	16-QAM
Channel spacing (Ω_0)	$2\pi\times$ 100 GHz
Number of channels (N)	50
WDM optical band	187.5 THz to 192.5 THz

of a standard standard single mode fiber (SMF) [18]. This corresponds to a loss of 0.19 dB km^{-1} at 190 THz. Here we present the results only for 6 channels, uniformly distributed within the WDM spectrum, which are enough to grasp the performance of the entire WDM grid. The signal input power per channel spans the range from −20 dBm to 0 dBm and Nyquist pulses were used. The numerical evaluation of the NLIN variance is based on Eq. (15) and implies the computation of the $X_{0,m,m}$ integrals for all collisions occurring among the channel under test and all the interfering channels. Note that this requires a three-step procedure. First, the Raman gain optimization problem is solved and the functions $f_B(z)$ are determined for all propagating signals. To this end, only the fiber length, the Raman gain coefficient, the WDM settings (i.e. the number and frequencies of the WDM channels), and the number of pumps need to be specified. The second step, the calculation of the time integrals within Eq. (13), is the most time-consuming section. This can be done once the input pulse shape, the frequency of the WDM channels, and the fiber dispersion are fixed. Note that the first and second steps are independent if the number and frequencies of the WDM channels are fixed. Finally, the third step is the integration over z of Eq. (13) to yield $X_{0,m,m}$.

The evaluation of the terms $X_{0,m,m}$ for a pair of adjacent channels is shown in Fig. 7 for all pumping schemes (CO, CT, and BI). The figure shows a great variation in the magnitude of the pulse collisions at different orders; in particular, incomplete collisions at the beginning and at the end of the fiber give weak contributions to the total noise. Fig. 8 is a plot of the ASE and NLIN powers as a function of the signal input power per channel. The figure confirms that the CO scheme typically presents a significantly lower ASE noise than the CT scheme, while having a greater amount of NLIN [19]. The difference in ASE performance is readily understood by considering the fact that in the CO scheme the highest gain is experienced by the signal close to the beginning of the fiber link, which yields a better ASE noise figure than in the CT scheme, where the highest gain is experienced towards the end the fiber link. Conversely, since the signal power along the fiber link on average is larger in CO scheme, as shown in Fig. 1, the NLPN variance is larger in the CO scheme than in the CT scheme.

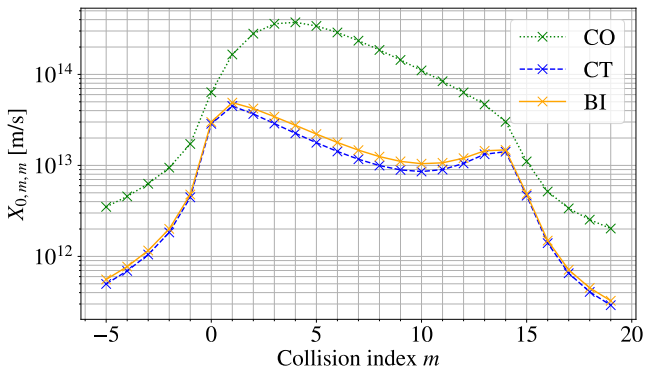

Fig. 7. Value of $X_{0,m,m}$ versus the collision index m for channels 1 and 2, for a signal input power per channel of −6 dBm. Values obtained by integration of Eq. (13).The CO scheme makes use of 4 co-propagating pumps, the CT scheme makes use of 4 counter-propagating pumps, and the BI scheme makes use of 2 co-propagating and 4 counter-propagating pumps.

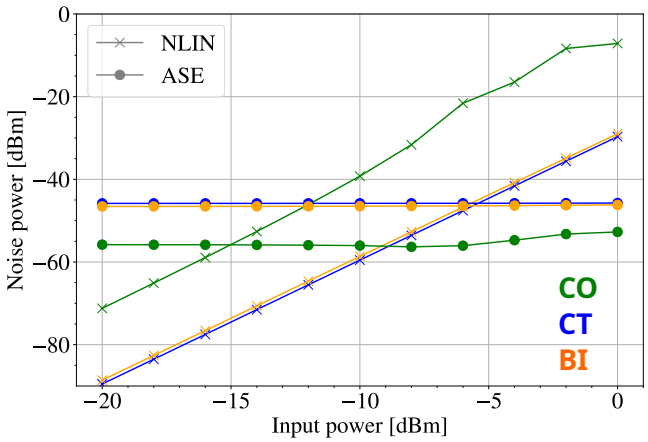

Fig. 8. Comparison between NLIN and ASE dependence on the signal input power per channel. The plotted values are the average of the results obtained for 6 equally spaced WDM channels. The CO scheme makes use of 4 co-propagating pumps, the CT scheme makes use of 4 counter-propagating pumps, and the BI scheme makes use of 2 co-propagating and 4 counter-propagating pumps.

Fig. 8 shows the known property of NLIN noise to increase with the cube of the signal input power per channel for all pumping schemes. Note also that, in the CO scheme, for large input power values, the NLIN and ASE noises tend to be affected by the strong nonlinear dynamics discussed in section II-A.

Let us now focus on the spectral properties of the noise. In [19], the possibility of spectral equalization of the OSNR in the presence of ASE only, using a bidirectional pumping scheme, has been shown. However, that approach is no longer valid as soon as NLIN is taken into consideration in the equalization. To demonstrate this we first set the conditions to achieve gain equalization in the CO, CT, and BI pumping schemes, for an input power of −14 dBm. The values of the input power and wavelengths of the pumps calculated by the optimization routine are reported in Table II. The calculation of ASE noise confirms the noise flattening, as shown in Fig. 9, where the OSNR variation over the spectrum is reduced from about 0.8 dB to about 0.1 dB. However, we notice that, independently from the input power, the total noise spectral profile is more heavily influenced by NLIN as shown in Fig. 10, where we plot the NLIN variance as a function of the channel wavelength for the three pumping configurations considered here, and for the reference case of an ideal distributed amplification (i.e. lossless propagation) as it results from [16]. In Fig. 10 input powers of −14 dBm and −6 dBm are considered. For the BI pumping scheme, NLIN dominates the spectral properties, with a variation over the spectrum of about 2 dB. It is known that the interference of adjacent channels is more relevant than the one due to channels far apart in frequency, and so the different power evolution of the mean signal power due to DRA might affect the spectral distribution of NLIN. In fact, from the plot, it can be also observed that there is a symmetry in the NLIN noise amplitude with respect to the center of the transmission band for all schemes with the exception of the co-propagating pumping scheme, that in fact present the larger asymmetry in the signal power evolutions.

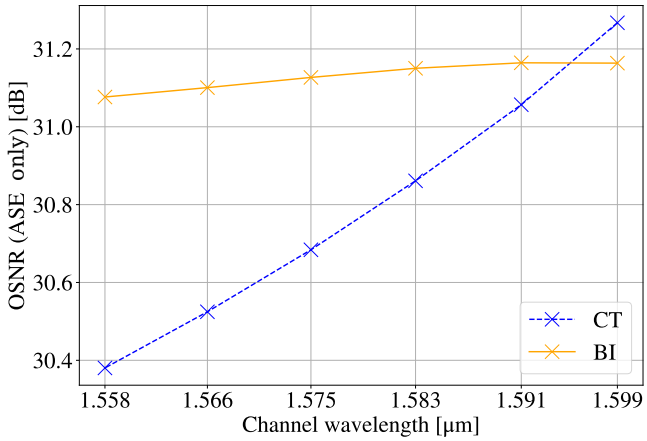

Fig. 9. The OSNR due to ASE only is plotted as a function of the channel wavelength for a signal input power per channel of −14 dBm. A weak dependence of OSNR is observed in the case of bidirectional pumping. The CT scheme makes use of 4 counter-propagating pumps, and the BI scheme makes use of 2 co-propagating and 4 counter-propagating pumps.

Some intuition on the BI and CT spectral distribution can be further obtained by considering the regime of large dispersion, although it describes accurately only long-haul links. In that approximation, assuming an ideal distributed amplification (i.e. lossless propagation) [16, 31], the term $X_{0,m,m}$ depends on the channel frequency spacing $X_{0,m,m}(k) \simeq 1/(\beta_2\Omega_0 k)$, because $\Omega = k\Omega_0$ where Ω_0 is the separation of two adjacent channels in the spectral domain and the integer k is the channel index difference. The total NLIN power is therefore proportional to the sum

$$P_{\mathrm{NLIN}} \propto \sum_{k\in I}\sum_{m} X^2_{0,m,m}(k) = \frac{L}{T}\frac{1}{|\beta_2\Omega_0|}\sum_{k\in I}\frac{1}{k} \qquad (28)$$

where I is the set of all the interfering channels index differences and $m < |\beta_2\Omega|L/T$ has been used to calculate the

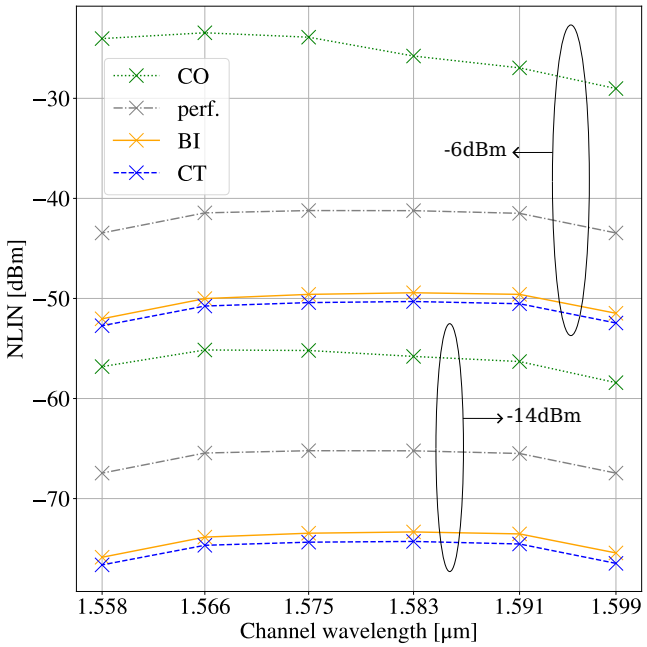

Fig. 10. The NLIN variance is plotted as a function of the channel wavelength for a signal input power per channel of −6 dBm (top set of lines) and −14 dBm (bottom set of lines). The CO scheme makes use of 4 co-propagating pumps, the CT scheme makes use of 4 counter-propagating pumps, the BI scheme makes use of 2 co-propagating and 4 counter-propagating pumps. Light grey curves (perf.) refer to the case of ideal Raman amplification, where the Raman gain equals the fiber loss at all propagation distances.

TABLE II
PUMP POWERS AND WAVELENGTHS USED IN FIG. 9 AND FOR THE CASE OF −14 dBm INPUT CHANNEL POWER OF FIG. 10

		Wavelength [μm]	**Power** [dBm]
CO		1.400	20.5
		1.450	20.2
		1.464	19.3
		1.504	19.1
CT		1.449	19.6
		1.465	17.3
		1.488	19.6
		1.514	14.5
BI	CO	1.481	10.2
		1.517	10.0
	CT	1.449	20.3
		1.464	18.3
		1.489	19.8
		1.515	13.9

sum for the index m. The last equation shows that the nearest channels have a greater weight in the total noise evaluation.

Finally, the OSNR of the channel or index i can be calculated as $\mathrm{OSNR}_i = P_i(z=L)/(N_i + P_{\mathrm{NLIN},i})$. In Fig. 11 we present the OSNR average over the 6 channels, as a function of the signal input power per channel. Our approach enables us to evaluate the optimal launching power regarding noise performance for each different pumping scheme. In particular, for CO the optimal signal input power per channel must be very low (about −16 dBm) while for the CT and BI cases, it is about the same and an order of magnitude larger than for the CO case (about −6 dBm). The input power values that optimize the generalized OSNR are known to be such that the NLIN power is 3 dB lower than ASE noise power [28]. They yield a maximum OSNR value of approximately 35 dB for all pumping schemes.

Note that the present analysis does not account for pump-to-signal relative intensity noise (RIN) transfer [19]. This noise contribution is known to be negligible in the CT scheme, but it can be relevant in the CO and BI schemes, unless pump lasers have negligible RIN. Therefore, our results apply to the case of ultra-low RIN pump lasers, similar to [25].

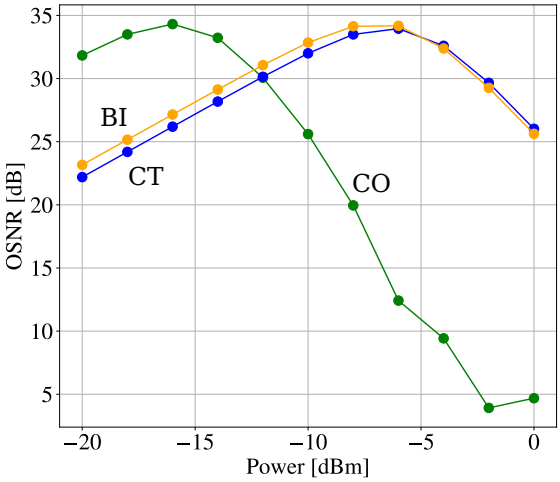

Fig. 11. Generalized OSNR versus channel input power. The plotted values are the average of the results obtained for 6 equally spaced WDM channels. The CO scheme makes use of 4 co-propagating pumps, the CT scheme makes use of 4 counter-propagating pumps, and the BI scheme makes use of 2 co-propagating and 4 counter-propagating pumps.

Finally, we evaluate the generalized OSNR for hybrid amplification schemes that yield per-channel full compensation of fiber losses. The contour plot in Fig. 12 shows the generalized OSNR as a function of the DRA target gain ranging between −6 dB and 0 dB (where the value of 0 dB describes the case of pure Raman amplification) and input powers ranging between −20 dBm and 0 dBm, for the CT (left) and CO (right) pumping schemes. Best performance is achieved in both cases for pure DRA, while no appreciable degradation is observed when the residual EDFA gain is between 3 and 4 dB. Our findings are somewhat consistent with previous studies based on GN models, showing that in the case of a single Raman pump, pure DRA is optimal in the CT scheme, and only slightly sub-optimal in the CO scheme [25, 32]. There, full compensation through DRA was optimal for CT pumping and only slightly sub-optimal for CO pumping.

IV. CONCLUSIONS

We presented an extension of the time-domain model for the NLIN that accounts for channel-dependent attenuation and gain in multi-pump Raman-amplified, polarization multiplexed coherent transmission links with various pumping schemes: co-propagating pumps, counter-propagating pumps, and bidirectional pumping. The model is also extended to account for signal-to-signal SRS interaction noise, which NLIN is found to

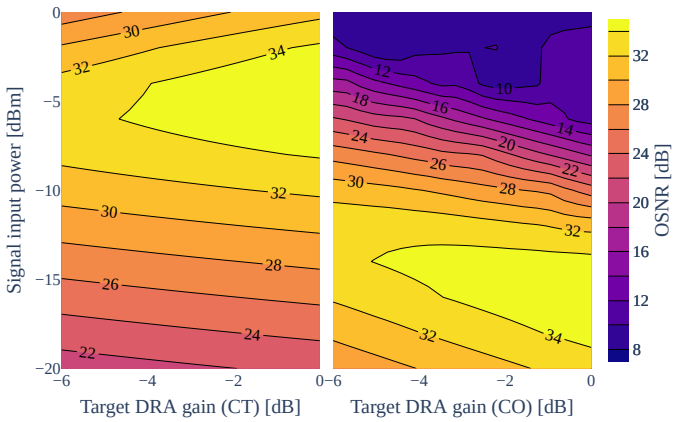

Fig. 12. OSNR plot for a hybrid amplification scenario. The DRA is set using our gain flattening algorithm to a target gain, and it is followed by an EDFA, which finalizes the loss compensation, and introduces additional ASE noise. OSNR values are obtained by averaging the values over 6 equally spaced channels. The CO scheme makes use of 4 co-propagating pumps, the CT scheme makes use of 4 counter-propagating pumps.

be practically negligible in the C-band. The numerical evaluation of the derived nonlinear noise variance expression shows that the NLIN has a spectral distribution similar to the case of ideal distributed fiber loss compensation, with the channels in the center of the grid more affected by nonlinear noise. The weak frequency dependence of amplified spontaneous emission in the presence of bidirectional pumping is shown to be overcome by the spectral variations of NLIN, in the regimes where the latter effect predominates. The counter-propagating and bi-directional pumping schemes are shown to have similar performance, which suggest that the latter should be preferred owing to its lower complexity. In the co-propagating scheme NLIN can show asymmetric variations with respect to the channel frequency position, due to the larger differences in the evolution of the channel signal powers. The co-propagating scheme, where the larget contribution to the NLIN is generated close to the beginning of the fiber link, is found to perform optimally at very low channel input powers. However, the exploitation of such optimal performance is hampered by other noise contributions, such as pump-to-signal intensity noise. Hybrid amplification schemes based on distributed Raman amplification and lumped EDFA amplification do not lead to better performances in terms of NLIN. Future development may involve the inclusion of NLIN estimation in the Raman amplifier design optimization, along with ASE noise. This may result in a comprehensive tool for systems design.

V. Acknowledgements

This work was partially supported by the European Union under the Italian National Recovery and Resilience Plan (NRRP) of NextGenerationEU, partnership on "Telecommunications of the Future" (PE0000001 - program "RESTART") and under project Vitality (CUP E13C22001060006), and by the Italian Ministry for Education, University and Research (MUR) through PRIN 2017-project 2017HP5KH7: Fiber Infrastructure for Research on Space-division multiplexed Transmission (FIRST).

References

[1] G. D. Rosa, S. Dris, and A. Richter, "Statistical quantification of nonlinear interference noise components in coherent systems", *Opt. Expr.*, vol. 28, no. 4, pp. 5436–5447, 2020.

[2] R.-J. Essiambre, G. Kramer, P. J. Winzer, G. J. Foschini, and B. Goebel, "Capacity limits of optical fiber networks", *J. Lightw. Technol.*, vol. 28, no. 4, pp. 662–701, 2010.

[3] R. Dar, M. Shtaif, and M. Feder, "New bounds on the capacity of the nonlinear fiber-optic channel", *Opt. Lett.*, vol. 39, no. 2, pp. 398–401, 2014.

[4] A. Mecozzi, and R.-J. Essiambre, "Nonlinear Shannon limit in pseudolinear coherent systems", *J. Lightw. Technol.*, vol. 30, no. 12, pp. 2011–2024, 2012.

[5] R. Dar, M. Feder, A. Mecozzi, and M. Shtaif, "Inter-channel nonlinear interference noise in WDM systems: Modeling and mitigation", *J. Lightw. Technol.*, vol. 33, no. 5, pp. 1044–1053, 2015.

[6] R. Dar, and P. J. Winzer, "Nonlinear interference mitigation: Methods and potential gain", *J. Lightw. Technol.*, vol. 35, no. 4, pp. 903–930, 2017.

[7] R. Dar, M. Feder, A. Mecozzi, and M. Shtaif, "Accumulation of nonlinear interference noise in fiber-optic systems", *Opt. Expr.*, vol. 22, no. 12, pp. 14 199–14 211, 2014.

[8] G. Bosco, R. Cigliutti, A. Nespola, A. Carena, V. Curri, F. Forghieri, Y. Yamamoto, T. Sasaki, Y. Jiang, and P. Poggiolini, "Experimental investigation of nonlinear interference accumulation in uncompensated links", *IEEE Photon. Technol. Lett.*, vol. 24, no. 14, pp. 1230–1232, 2012.

[9] O. Golani, D. Elson, D. Lavery, L. Galdino, R. Killey, P. Bayvel, and M. Shtaif, "Experimental characterization of the time correlation properties of nonlinear interference noise", in 2017 *European Conf. Opt. Commun. (ECOC)*, 2017, pp. 1–3.

[10] N. V. Gurkin, O. E. Nanii, A. G. Novikov, S. O. Plaksin, V. N. Treshchikov, and R. R. Ubaidullaev, "Nonlinear interference noise in communication lines with the DP-QPSK modulation format", *Quantum Electronics*, vol. 43, no. 6, p. 550, 2013.

[11] O. Golani, M. Feder, and M. Shtaif, "Kalman-MLSE equalization for NLIN mitigation", *J. Lightw. Technol.*, vol. 36, no. 12, pp. 2541–2550, 2018.

[12] P. Poggiolini, A. Carena, V. Curri, G. Bosco, and F. Forghieri, "Analytical modeling of nonlinear propagation in uncompensated optical transmission links", *IEEE Photon. Technol. Lett.*, vol. 23, no. 11, pp. 742–744, 2011.

[13] P. Poggiolini, G. Bosco, A. Carena, V. Curri, Y. Jiang, and F. Forghieri, "A detailed analytical derivation of the GN model of non-linear interference in coherent optical transmission systems", 2014. arXiv: 1209.0394.

[14] P. Poggiolini, "A generalized GN-model closed-form formula", 2018. arXiv: 1810.06545.

[15] A. Carena, G. Bosco, V. Curri, Y. Jiang, P. Poggiolini, and F. Forghieri, "EGN model of non-linear fiber propagation", *Opt. Expr.*, vol. 22, no. 13, pp. 16 335–16 362, 2014.

[16] R. Dar, M. Feder, A. Mecozzi, and M. Shtaif, "Properties of nonlinear noise in long, dispersion-uncompensated fiber links", *Opt. Expr.*, vol. 21, no. 22, p. 25 685, 2013.

[17] R. Dar, M. Feder, A. Mecozzi, and M. Shtaif, "Pulse Collision Picture of Inter-Channel Nonlinear Interference in Fiber-Optic Communications", *J. Lightw. Technol.*, vol. 34, no. 2, 2016.

[18] G. Marcon, A. Galtarossa, L. Palmieri, and M. Santagiustina, "Model aware deep learning method for Raman amplification in few-mode fibers", *J. Lightw. Technol.*, vol. 39, no. 5, pp. 1371–1380, 2021.

[19] J. Bromage, "Raman amplification for fiber communications systems", *J. Lightw. Technol.*, vol. 22, no. 1, pp. 79–93, 2004.

[20] K.-P. Ho, "Statistical properties of stimulated Raman crosstalk in WDM systems", *J. Lightw. Technol.*, vol. 18, no. 7, pp. 915–921, 2000.

[21] D. Semrau, G. Saavedra, D. Lavery, R. I. Killey, and P. Bayvel, "A closed-form expression to evaluate nonlinear interference in Raman-amplified links", *J. Lightw. Technol.*, vol. 35, no. 19, pp. 4316–4328, 2017.

[22] H. Rabbani, G. Liga, V. Oliari, L. Beygi, E. Agrell, M. Karlsson, and A. Alvarado, "An improved model of nonlinear fiber propagation in the presence of Kerr nonlinearity and stimulated Raman scattering", 2020. arXiv: 1909.08714.

[23] W. Wang, J. Zhao, Z. Yang, C. Li, Z. Wang, L. Yu, and R. Mi, "Amplified spontaneous emission and Rayleigh scattering in few-mode fiber Raman amplifiers", *IEEE Photon. Technol. Lett.*, vol. 29, no. 14, pp. 1159–1162, 2017.

[24] A. Pizzinat, M. Santagiustina, and C. Schivo, "Impact of hybrid EDFA-distributed Raman amplification on a 4 x 40-Gb/s WDM optical communication system", *Phot. Tech. Lett.* 15, 341–343, 2003.

[25] V. Curri and A. Carena, "Merit of Raman Pumping in Uniform and Uncompensated Links Supporting NyWDM Transmission", *J. Lightw. Technol.* 34, 554–565, 2016.

[26] G. P. Agrawal, Nonlinear fiber optics. Academic Press, 2013.

[27] P. Poggiolini, Y. Jiang, "Recent Advances in the Modeling of the Impact of Nonlinear Fiber Propagation Effects on Uncompensated Coherent Transmission Systems", *J. Lightw. Technol.*, vol. 35, no. 3, pp. 458-480, 2017.

[28] G. Bosco, A. Carena, R. Cigliutti, V. Curri, P. Poggiolini, and F. Forghieri, "Performance prediction for WDM PM-QPSK transmission over uncompensated links", in *Opt. Fiber. Commun. Conf. (OFC)* 1–3 2011.

[29] A. Nespola, L. Bertignono, G. Bosco, A. Carena, P. Poggiolini, and F. Forghieri, "Independence of the Impact of Inter-Channel Non-Linear Effects on Modulation Format and System Implications", in 2017 *European Conf. Opt. Commun. (ECOC)*, 2017.

[30] T. Fehenberger, M. P. Yankov, L. Barletta, and N. Haink, "Compensation of XPM interference by blind tracking of the nonlinear phase in WDM systems with QAM input", in 2015 *European Conf. Opt. Commun. (ECOC)*, 2015.

[31] A. Papoulis, "Pulse compression, fiber communications, and diffraction: A unified approach", *J. Opt. Soc. Am.* A, vol. 11, no. 1, pp. 3–13, 1994.

[32] V. Curri, A. Carena, P. Poggiolini, G. Bosco, and F. Forghieri "Extension and validation of the GN model for non-linear interference to uncompensated links using Raman amplification" *Opt. Expr.*, vol. 21, no. 3, pp. 3308-3317, 2013.